Research Square

Preprints are preliminary reports that have not undergone peer review.
They should not be considered conclusive, used to inform clinical practice,
or referenced by the media as validated information.

Structural and aggregation effects on the thermoresponsiveness of PDMAEMA-b-PS copolymers synthesized via one-pot RAFT polymerization

Vinicios Santiago Araujo
Universidade de São Paulo
Fábio Herbst Florenzano
fhfloren@usp.br

Universidade de São Paulo

Research Article

Keywords: PDMAEMA-b-PS, RAFT, Polymer self-assembly, LCST

Posted Date: November 13th, 2026

DOI: https://doi.org/10.21203/rs.3.rs-11515324/v1

License: This work is licensed under a Creative Commons Attribution 4.0 International License.
Read Full License

Additional Declarations: No competing interests reported.

Structural and aggregation effects on the thermoresponsiveness of PDMAEMA-*b*-PS copolymers synthesized via one-pot RAFT polymerization

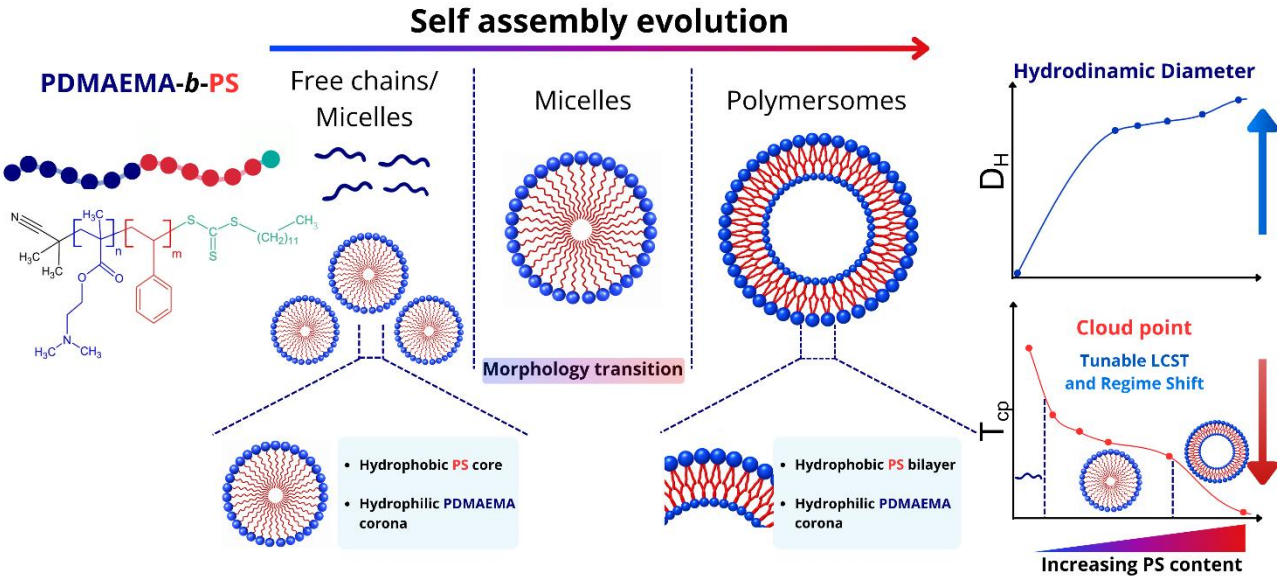
Vinicios Santiago Araujo[1] · **Fábio Herbst Florenzano**[1]

Abstract

Thermoresponsive copolymers have been widely applied in many fields such as antimicrobial coatings, controlled drug delivery, and antifouling smart coatings. However, many applications require fine-tuning of the thermal behavior, which can be achieved by tailoring the material's composition and architecture. For example, for amphiphilic block copolymers with a lower critical solution temperature (LCST), thermoresponsiveness strongly depends on the hydrophobic/hydrophilic ratio. Additionally, because block solubility in aqueous media differs considerably, self–assembly can occur, producing highly ordered structures such as micelles and polymersomes. This change in aggregation also affects the thermal response by altering the local polarity around the responsive units. Hence, the overall composition of the polymeric material and its aggregation contribute simultaneously to thermoresponsiveness. Here, Reversible Addition-Fragmentation Chain Transfer (RAFT) was used to synthesize two series of poly[N,N-(dimethylamino)ethyl methacrylate)]-*block*-polystyrene (PDMAEMA-*b*-PS) with increasing PS fraction and low molecular dispersity (Đ < 1,5) through a one-pot polymerization, aiming to evaluate the aggregation effects on the thermal behavior. Two distinct thermoresponsive homopolymers, $PDMAEMA_{93}$ and $PDMAEMA_{131}$, were used for each series, enabling the synthesis of 17 different materials, which were thoroughly characterized. Cloud point temperature (T_{cp}) and aggregation properties were assessed in aqueous media via UV-Visible turbidimetry and DLS, respectively. PDMAEMA-*b*-PS copolymers showed a swift decrease in T_{cp} with minor PS block additions followed by another aggregation transition at higher hydrophobic/hydrophilic ratios with an abrupt drop in the cloud point temperature, as the PS content increased. These results indicate that the system aggregation status must be considered to understand how thermoresponsiveness depends on the copolymer's overall polarity.

Keywords PDMAEMA-*b*-PS; RAFT; Polymer self-assembly; LCST

Graphical Abstract



Fabio Herbst Florenzano

fhfloren@usp.br

1 Department of Materials Engineering, Engineering School of Lorena, University of São Paulo, Lorena, 12602-810 São Paulo, Brazil

Introduction

Thermal response is described by a binodal transition curve that separates monophasic and biphasic equilibrium regions in a solvent-polymer phase diagram [1]. The critical point of the curve may either correspond to a minimum or a maximum, indicating the lower (LCST) and upper (UCST) critical solution temperatures, respectively. In both cases, the temperature at which the phase transition occurs is governed by the Gibbs free energy equation for mixing ($\Delta G_m = \Delta H_m - T\Delta S_m$) and indicates the cloud point (T_{cp}) at a given concentration [2]. Consequently, thermoresponsive polymer systems presenting an LCST may reversibly modify their physicochemical properties in response to temperature stimuli [3]. These smart materials have been harnessed in several applications such as nanocarriers for drug delivery [4–6], tissue engineering [7, 8], antimicrobial, self-healing, and antifouling surfaces [9–12].

Structural modifications can precisely tailor thermoresponsive behavior, particularly through polymeric architecture and polymer-solvent interactions [13–15]. Poly[N,N-(dimethylamino)ethyl methacrylate] (PDMAEMA), a cationic polyelectrolyte, shows an LCST-type response that is also strongly pH-dependent due to protonation of the tertiary amine groups in aqueous media (pKa ~ 7.5) [16, 17], which accounts for the enthalpic contribution of ΔG_m [18]. The dual-responsive property of PDMAEMA is interesting for broadening the range of applications since above its pKa, PDMAEMA is mostly deprotonated and undergoes a sharp coil-to-globule transition at lower temperatures. Also, the LCST of PDMAEMA-based copolymers can be modulated by incorporating hydrophobic blocks such as polystyrene (PS), poly(methyl methacrylate), and 2-(2-methoxyethoxy)ethyl methacrylate into the hydrophilic polymer chains [19–21].

Poly[N,N-(dimethylamino)ethyl methacrylate)]-*block*-polystyrene (PDMAEMA-*b*-PS) copolymers have exhibited applications in several fields: antimicrobial materials, active coating, templating, and self–assembled nanoparticles for controlled drug delivery [22–26], along with their thermoresponsive behavior. The amphiphilic nature of PDMAEMA-*b*-PS provides a variety of aggregate morphologies in water, including micelles and polymersomes, depending on the relative composition, architecture, and pH [21]. More importantly, the rigid polystyrene block forms aggregate cores, enabling efficient encapsulation and controlled drug release due to good colloidal stability [24, 27]. In addition, the hydrophobic/hydrophilic ratio (r) significantly alters both the thermal response and self-assembly dynamics [28]. For instance, Han et al. [29] showed that the increase in relative PDMAEMA block sizes in poly[N,N-(dimethylamino)ethyl methacrylate)]-*b*-poly(acrylic acid) (PDMAEMA-*b*-PAA) copolymers led to the formation of micellar aggregates, while PAA-rich copolymers shifted this tendency towards vesicular morphologies. Higher PDMAEMA contents also increased the LCST of the copolymer under the same conditions, highlighting the structural impacts on the copolymer's thermoresponsiveness and aggregation behavior.

Although many studies show a correlation between the polar/apolar ratio and the LCST of different copolymers in aqueous media [18, 29, 30], the impact of aggregation on thermal behavior is frequently overlooked, and a clear relationship has not been established. This is due to multiple factors: different aggregate structures may coexist under the same conditions, as reported by Gjerde et al. [31]; complex inter- and intramolecular interactions between polymer chains [31]; and kinetic effects (aggregate formation and growth) are among some of them [32]. Aggregate formation substantially changes the environment of the thermoresponsive block, including polarity and local pH, factors that usually strongly affect thermoresponse [33]. Therefore, self-assembly is expected to alter how an amphiphilic copolymer responds to temperature. This work aims to investigate how the hydrophilic/hydrophobic ratio and the aggregation state simultaneously affect the cloud point of PDMAEMA-*b*-PS copolymers.

To systematically study the effect of the polar/apolar ratio and aggregation, precise control of the copolymer structure is needed. A reliable way to obtain amphiphilic block copolymers with systematic changes in block sizes is reversible deactivation radical polymerization (RDRP) [34–36]. Because it works with a wide range of monomers and provides rigorous control over molar mass and molecular dispersity (Đ), Reversible Addition–Fragmentation Chain Transfer (RAFT) polymerization is widely used to synthesize well-defined stimuli-responsive copolymers [2, 37, 38]. In the present work, RAFT polymerization was applied to synthesize, in one pot, two series of PDMAEMA-*b*-PS copolymers, each with the same hydrophilic PDMAEMA macroCTA and increasing hydrophobic content. The two copolymer series, with different polarities, allowed simultaneous study of aggregation and thermoresponsiveness, shedding light on how aggregation affects the LCST, besides overall polarity. Therefore, this study aims to better understand how hydrophobicity and aggregation status jointly affect the LCST response of PDMAEMA copolymers.

Materials

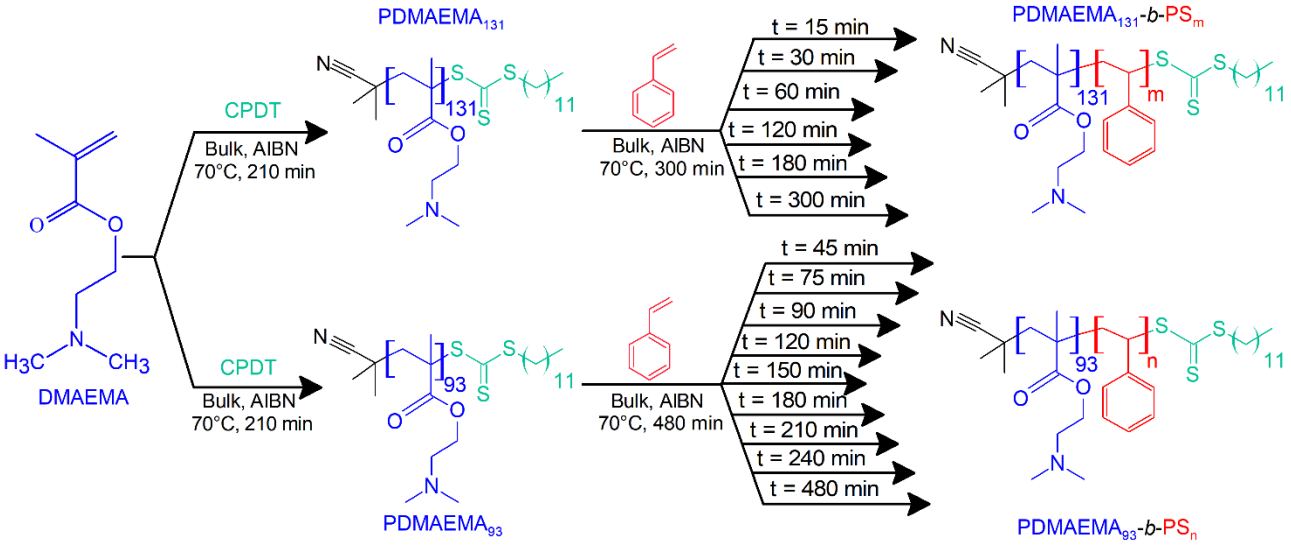
RAFT agent 2-cyano-2-propyl dodecyl trithiocarbonate (CPDT), deuterated chloroform ($CDCL_3$), monohydrate monosodium phosphate ($NaH_2PO_4.H_2O$, 99%), styrene (98%) and dimethyl-2-(aminoethyl) methacrylate (DMAEMA, 98%) were obtained from Sigma - Aldrich. Monomethyl ether hydroquinone (MEHQ) removal from monomers was performed through filtration in an anhydrous aluminum oxide (Al_2O_3) column at a 1:5 oxide-to-monomer mass ratio. 2,2′-Azobis(2-methylpropionitrile) (AIBN) was obtained from Sigma-Aldrich and recrystallized from ethanol. Milli-Q (Millipore Co.) water was used to prepare all aqueous solutions. Hexane (98,5%), 1,4–dioxane (99%), and THF (99%) were acquired from Synth. All remaining chemicals were used as received from Sigma-Aldrich.

RAFT Synthesis of PDMAEMA MacroCTAs

PDMAEMA$_{131}$ and PDMAEMA$_{93}$ PDMAEMA homopolymers were produced to be used as macroCTA to generate one series each. PDMAEMA$_{131}$ was synthesized in bulk using CPDT as the chain transfer agent and a 5:1 [CTA]:[AIBN] ratio. In a 100 mL three-necked round-bottom flask, DMAEMA (27.96 g, 178 mmol), CPDT (0.3283 g, 0.95 mmol), and AIBN (0.0317 g, 0.19 mmol) were added under vigorous stirring in a glycerin bath at 70 °C. The atmosphere was purged with argon at 30 min, and the reaction was initiated with AIBN. Samples were taken for kinetic measurements of the average molar mass (M_n) via SEC. The same procedure was repeated for PDMAEMA$_{93}$ homopolymer, using different quantities of DMAEMA (30.01 g, 191 mmol), CPDT (0.3511 g, 1.02 mmol) and a 0.5 mL solution of AIBN (0.0317 g, 0.205 mmol) in 1,4–dioxane. The homopolymers were further purified three times by solubilization–reprecipitation using THF and hexane, and then dried under vacuum for 2 h at 30 °C.

One-pot RAFT synthesis of PDMAEMA-*b*-PS series

PDMAEMA$_{93}$ and PDMAEMA$_{131}$ macroCTAs were used separately to synthesize two series of PDMAEMA-*b*-PS copolymers with increasing hydrophobic block content in one-pot reactions. For PDMAEMA$_{131}$-*b*-PS$_m$ series production, styrene (109.75 g, 1.05 mol), PDMAEMA$_{131}$ (10.00 g, 0.488 mmol) and a 0.5 mL solution of AIBN (0.0117 g, 0.07 mmol) in 1,4-dioxane were added in a 250 mL three-necked round-bottom flask under inert Ar atmosphere and magnetic stirring at 70 °C. 8 mL aliquots were taken at t = 15, 30, 60, 120 and 180 min and the reaction was ended after 5 hours. Similarly, PDMAEMA$_{93}$-*b*-PS$_n$ series was synthesized using styrene (137.42 g, 1.32 mol), PDMAEMA$_{93}$ (10.00 g, 0.688 mmol) and a 0.5 mL solution of AIBN (0.0226 g, 0.137 mmol) in 1,4-dioxane. The reaction was carried out for 8 hours, and aliquots were taken at t = 45, 75, 90, 120, 150, 180, 210, and 240 min as depicted in Scheme **1**. The aliquots taken at different times were individually purified using the same process described for the MacroCTA, yielding materials with the same PDMAEMA block and increasing PS content. All materials were dried under vacuum at 30 °C for 1 hour.



Scheme 1: One-pot RAFT Synthesis of PDMAEMA$_{131}$-*b*-PS$_m$ and PDMAEMA$_{93}$-*b*-PS$_n$ copolymers produced from PDMAEMA$_{131}$ and PDMAEMA$_{93}$ macroCTAs, respectively. *m* and *n* represent the PS block sizes for both copolymer series determined through SEC and ^{1}H-NMR.

Molecular Characterization

Number-average molecular mass (M_n) and molecular dispersity (Đ) of all synthesized materials were evaluated by Size Exclusion Chromatography (SEC) using THF/Triethylamine (0.3% v/v) as the mobile phase. A Shimadzu Prominence series chromatographic system was used, with an RID-10A refractive index detector, two Phenogel columns (pore sizes of 10^4 Å and 10^6 Å), a SIL-20A HT autosampler, and a CTO20A oven set to 35 °C. Samples were dissolved in the mobile phase and subsequently filtered through a 0.22 µm PTFE syringe filter. The flow rate was set to 0.8 mL.min^{-1}, and the injection volume was 50 µL. A ReadyCal poly (methyl methacrylate) standards kit (Sigma-Aldrich) ranging from 800 to 1.82 x 10^6 g mol^{-1} was used for calibration. Therefore, all molar masses indicated here are relative and equivalent to poly(methyl methacrylate) linear polymers.

^{1}H-NMR spectroscopy of homopolymers and copolymers was carried out on a Bruker DPX300 spectrometer at 300 MHz. Samples were prepared via solubilization in deuterated chloroform ($CDCl_3$), and the probe temperature was set to 25 °C. Tetramethylsilane (TMS) served as the reference.

Thermal behavior and self-assembly analysis

Cloud point evaluation was performed using a Thermo Scientific Evolution 201 UV/Vis Spectrophotometer equipped with a PCCU1 Peltier. (Co)polymer solutions at 10 mg.mL^{-1} in THF were slowly dissolved in 5 mL of 50 mmol.L^{-1} phosphate buffer solution (pH 7.8) under vigorous agitation, resulting in a final concentration of 0.2 mg.mL^{-1}. Samples were heated at 0.1°C/s with magnetic stirring from 40 to 75°C. For each run, λ = 450 nm, and we calculated the cloud point using the onset method, that considers the intersection of the baseline and the tangent to the transmittance decay in the transmittance versus temperature graph.

Aggregate sizes (D_H) and polydispersity indexes (PDI) were determined via dynamic light scattering (DLS) with the use of a ZetaPals equipment provided by Brookhaven Instruments Corporation. Analyses were performed at room temperature with an incident radiation of 660 nm. Polymer dispersions in phosphate buffer solution (0.2 mg mL^{-1}) were prepared as described above and filtered through a 0.22 µm Millipore PTFE syringe filter. Samples underwent 5 runs of 1 minute each.

Results

Polymer structural characterization

RAFT polymerization yielded 2 PDMAEMA homopolymers and 15 PDMAEMA-*b*-PS copolymers with narrow molar mass distributions and distinct hydrophobic segment sizes (Table **1**). Both PDMAEMA$_{93}$ (M_n = 14.5 kg/mol and Đ = 1.23) and PDMAEMA$_{131}$ (M_n = 20.5 kg/mol and Đ = 1.17) macroCTAs presented similar polymerization behaviors, with increasing relative peak areas (Fig. **1**a and **1**b) as molecular dispersity decreased (Fig. **2**a and **2**b). This is observed in RAFT-mediated polymerizations, as reaction equilibria are fully established during mid-stages and dispersity tends to reduce [34, 35, 39].

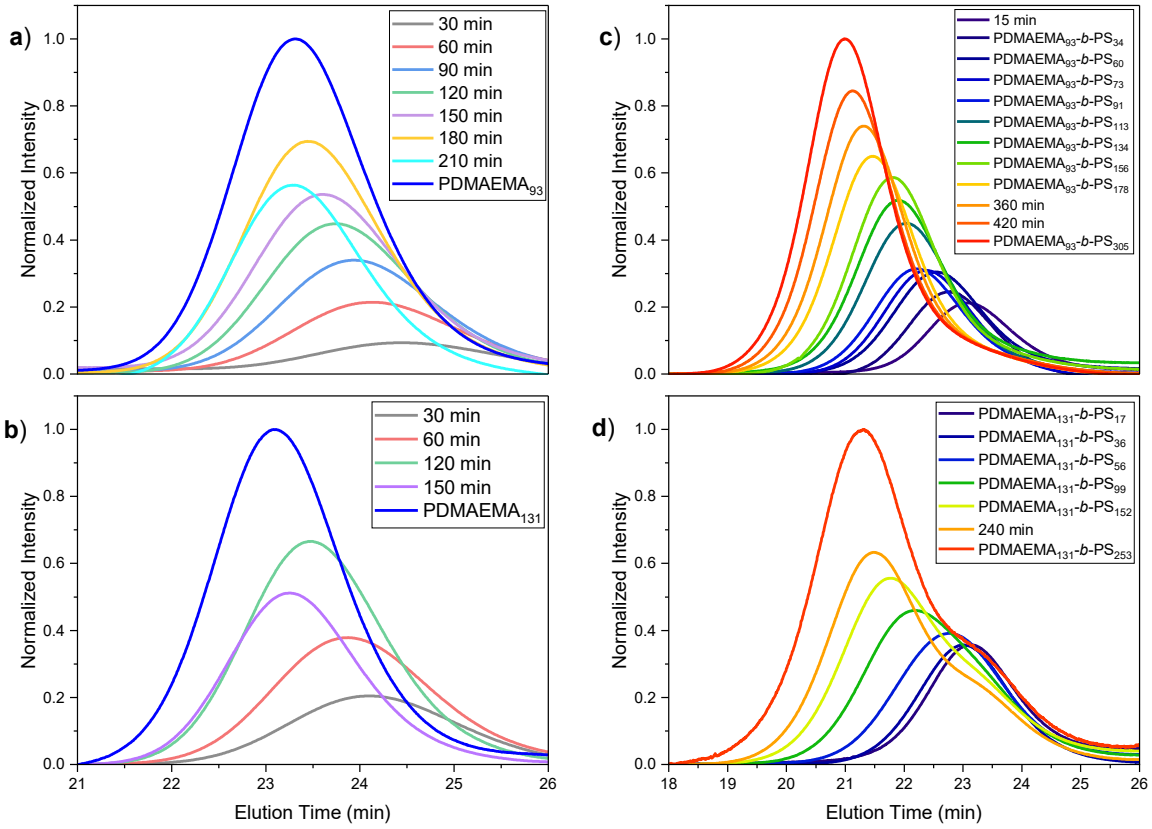


Fig. 1 SEC chromatograms of the materials during RAFT polymerizations: a) PDMAEMA$_{93}$, b) PDMAEMA$_{93}$-*b*-PS$_n$, c) PDMAEMA$_{131}$ and d) PDMAEMA$_{131}$-*b*-PS$_m$ RAFT

One-pot block copolymerization of PS with PDMAEMA$_{93}$ and PDMAEMA$_{131}$ produced PDMAEMA-*b*-PS materials with a wide range of compositions, from M_n = 23.2 kg/mol to M_n = 58.2 kg/mol, with Đ < 1.5 in all cases. Fig. **1**c and **1**d show that peak area increases for both the PDMAEMA$_{93}$-*b*-PS$_n$ and PDMAEMA$_{131}$-*b*-PS$_m$ series as the signal shifts to lower retention times during the reaction. This behavior indicates successful hydrophobic block incorporation since M_n progressively increases (Fig. **2**c and **2**d), as expected for controlled RAFT polymerization. Additional aliquots, not used for cloud point tests, were taken at t = 15, 360, and 420 min to monitor the reaction during PDMAEMA$_{93}$-*b*-PS$_n$ synthesis. SEC analysis of the PDMAEMA$_{131}$-*b*-PS$_m$ series revealed a secondary population, indicated by peak tailing at

low molecular weights, suggesting dead-chain formation [40]. As a result, Fig. **2**c shows relatively constant Đ throughout $PDMAEMA_{93}$-*b*-PS_n synthesis, while Fig. **2**d shows increasing dispersity for the $PDMAEMA_{131}$-*b*-PS_m series, though it remains below 1.5.

Table 1. Molecular characterization of PDMAEMA and PDMAEMA-*b*-PS materials after purification

Polymer	t[a] (min)	M_n[b] (kg/mol)	Đ[b]	f_{PS}:$f_{PDMAEMA}$[c]
$PDMAEMA_{93}$	-	14.5	1.23	0
$PDMAEMA_{93}$-*b*-PS_{34}	45	23.7	1.37	0.366
$PDMAEMA_{93}$-*b*-PS_{60}	75	24.3	1.26	0.645
$PDMAEMA_{93}$-*b*-PS_{73}	90	29.2	1.23	0.785
$PDMAEMA_{93}$-*b*-PS_{91}	120	32.9	1.25	0.978
$PDMAEMA_{93}$-*b*-PS_{113}	150	35.3	1.23	1.215
$PDMAEMA_{93}$-*b*-PS_{134}	180	38.9	1.25	1.441
$PDMAEMA_{93}$-*b*-PS_{156}	210	40.2	1.22	1.677
$PDMAEMA_{93}$-*b*-PS_{178}	300	49.6	1.29	1.914
$PDMAEMA_{93}$-*b*-PS_{305}	480	58.2	1.23	3.280
$PDMAEMA_{131}$	-	20.5	1.17	0
$PDMAEMA_{131}$-*b*-PS_{17}	15	23.2	1.25	0.130
$PDMAEMA_{131}$-*b*-PS_{36}	30	24	1.29	0.275
$PDMAEMA_{131}$-*b*-PS_{56}	60	28.8	1.27	0.427
$PDMAEMA_{131}$-*b*-PS_{99}	120	33.5	1.33	0.756
$PDMAEMA_{131}$-*b*-PS_{152}	180	39.1	1.32	1.160
$PDMAEMA_{131}$-*b*-PS_{253}	300	46.2	1.44	1.931

[a]Reaction times during copolymer aliquot removal. [b] Number-average molar mass (M_n) and molecular dispersity (Đ) obtained by SEC. [c]Hydrophobic/hydrophilic molar ratios determined from relative peak intensities via ^1H – NMR $\left(\frac{f_{PS}}{f_{PDMAEMA}} = \frac{I_{\delta=6.3-7.2\ ppm}}{I_{\delta=2.3\ ppm}} . \frac{n^H_{DMAEMA}}{n^H_{Styrene}}\right)$, where $I_{\delta\ =\ 6.3\ -\ 7.2\ ppm}$, $I_{\delta\ =\ 2.3\ ppm}$ correspond to the intensities of the aromatic and CH_3-N signals, respectively. $n^H_{Styrene}$ and n^H_{DMAEMA} are related to the contributing protons for each of these signals in the spectra.

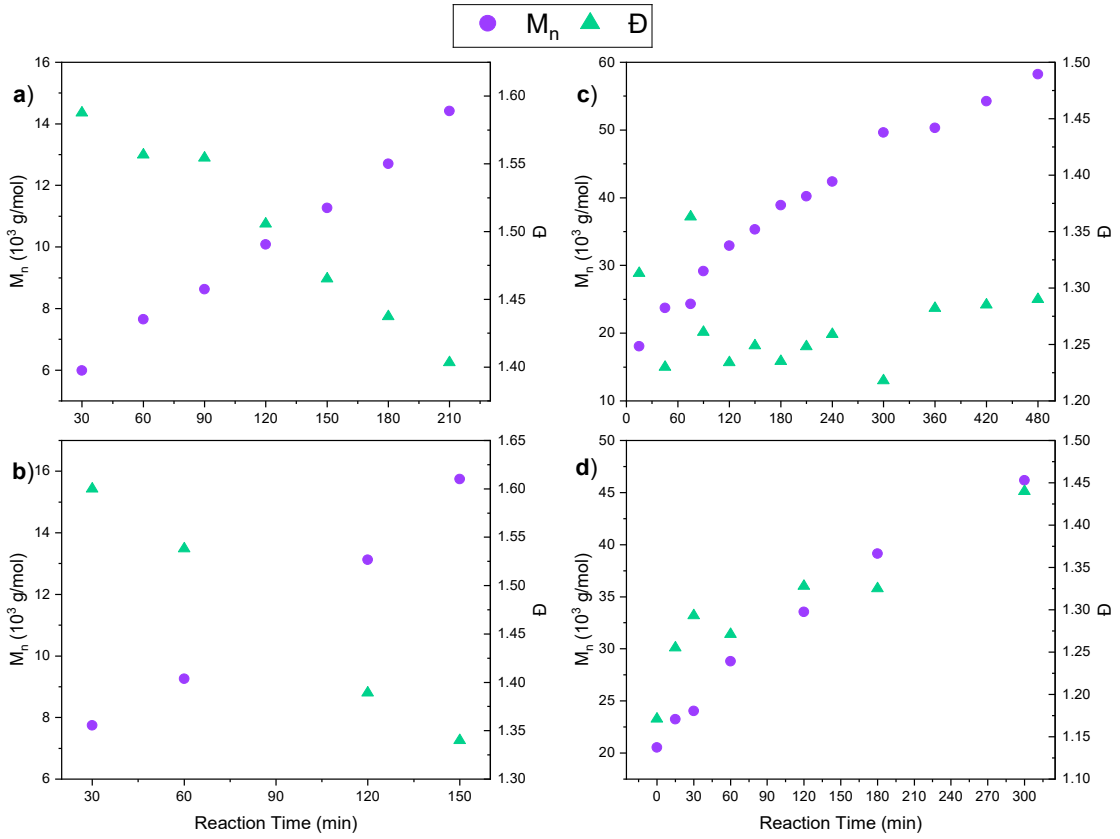


Fig. 2 Molecular dispersity (Đ) and M_n acquired from SEC during the synthesis of a) $PDMAEMA_{93}$, b) $PDMAEMA_{93}$-*b*-PS_n, c) $PDMAEMA_{131}$ and d) $PDMAEMA_{131}$-*b*-PS_m

Since hydrophobic/hydrophilic balance directly impacts self-assembly morphologies and thermal behavior [41–44], ^{1}H-NMR was used to determine the relative composition of the copolymers. Fig**. 3** shows a typical PDMAEMA-*b*-PS spectrum, acquired for $PDMAEMA_{131}$-*b*-PS_{253}. Block molar proportions (f_{PS}:$f_{PDMAEMA}$ in Table **1**) could be determined from the integral values of the aromatic proton signals from 6.3 to 7.2 ppm and CH_3-N signal near δ = 2.3 ppm. Fig**. 3**a and **3**b show increasing aromatic hydrogen signals as aliquot removal time progressed for $PDMAEMA_{93}$-*b*-PS_n and $PDMAEMA_{131}$-*b*-PS_m, respectively, consistent with the growth of the hydrophobic fraction in the copolymer chains. In some cases (see Supplementary Information), a minor signal at δ = 3.60 ppm was observed, corresponding to two protons of 2-dimethylaminoethanol (CH2-OH in Fig**. 3**), a PDMAEMA hydrolysis byproduct [45]. A doublet of doublets around δ = 6.75 ppm (vinylic protons) also indicated residual monomers after purification [46].

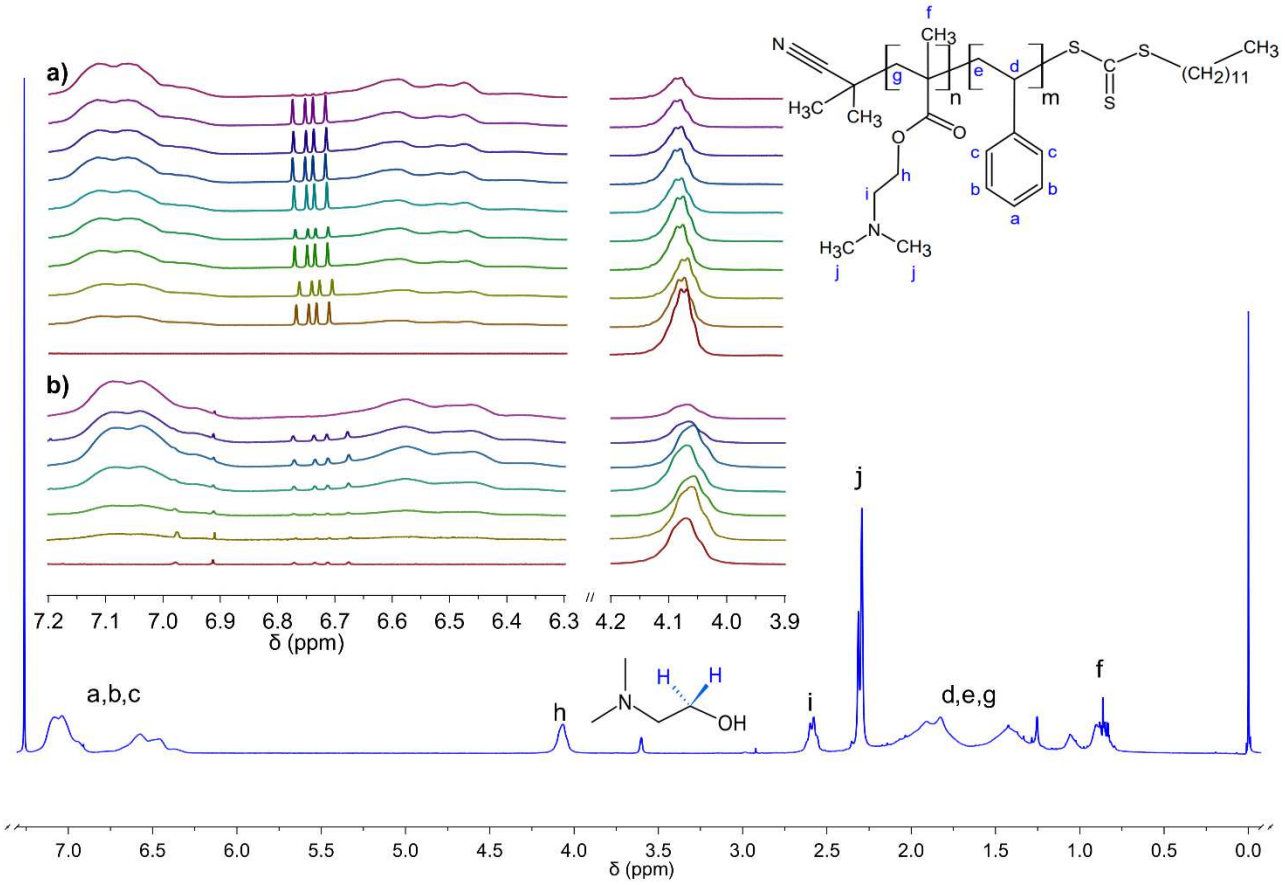


Fig. 3 ^{1}H – NMR spectrum of PDMAEMA-*b*-PS in $CDCl_3$ depicting the increase in overall hydrophobicity for a) $PDMAEMA_{93}$-*b*-PS_n and b) $PDMAEMA_{131}$-*b*-PS_m series. A pronounced reduction in the ratio between CH_2-O at δ = 4.07 ppm and aromatic protons signals (7.1 ppm region) is observed.

Thermoresponsive and aggregation behaviors

Cloud point measurements were carried out to evaluate the effects of gradual hydrophobic block insertion into the polymer chains. At low temperatures is governed by strong hydrogen bonding between PDMAEMA amine groups and water molecules. When temperature rises, hydrophilic interactions weaken, and phase separation occurs, leading to a pronounced coil-to-globule transition. Thus, increasing PS content is expected to promote phase separation at lower temperatures once overall hydrophilicity and the total hydrogen bonds decrease [21, 47, 48]. Fig. **4** shows this effect: transmittance drops at lower temperatures as PS content increases. Fig. **5** shows the cloud point temperatures of all materials.

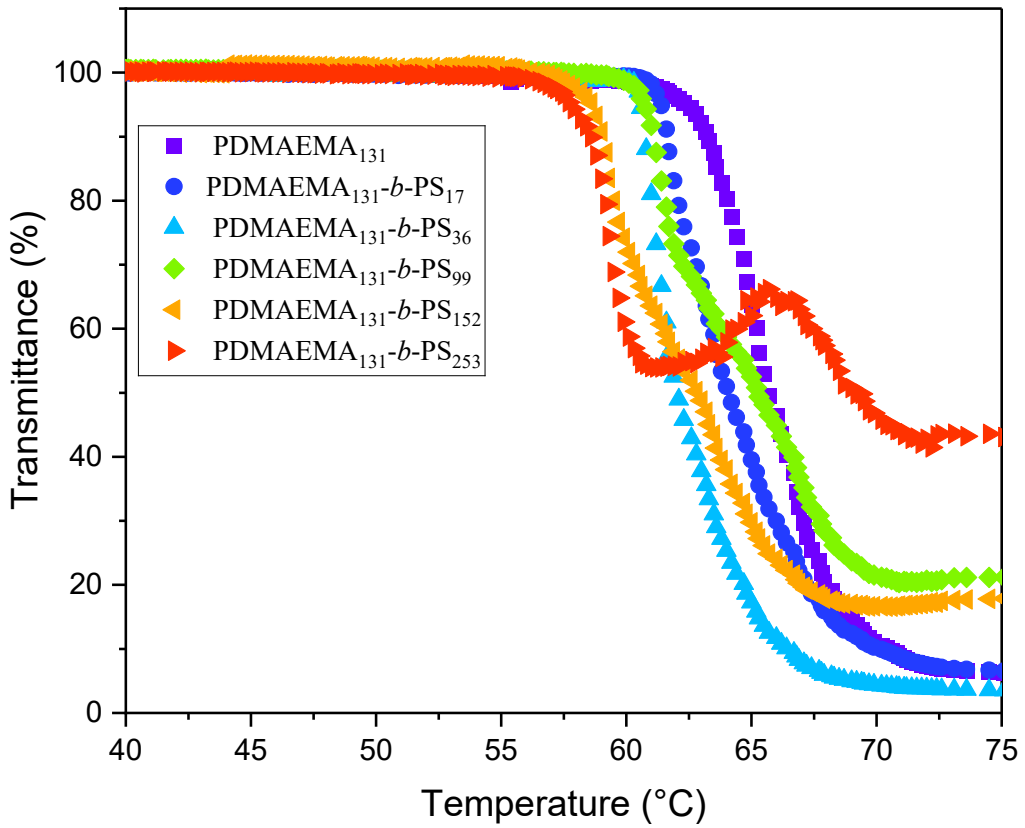


Fig. 4. Transmittance of $PDMAEMA_{131}$ (purple squares), $PDMAEMA_{131}$-*b*-PS_{17} (blue circles), $PDMAEMA_{131}$-*b*-PS_{36} (blue triangles), $PDMAEMA_{131}$-*b*-PS_{99} (green diamonds), $PDMAEMA_{131}$-*b*-PS_{152} (orange triangles) and $PDMAEMA_{131}$-*b*-PS_{253} (red triangles) in phosphate buffer solution, pH = 7.8. The transmittance curves for the remaining polymers of $PDMAEMA_{93}$-*b*-PS_n and $PDMAEMA_{131}$-*b*-PS_m are displayed in the supplementary information.

Fig. **5**a and Fig. **5**b show the decrease in T_{cp} as styrene is gradually introduced into the $PDMAEMA_{93}$ and $PDMAEMA_{131}$ polymer chains, respectively. Both homopolymers showed the highest cloud point temperatures (T_{cp} = 61°C and T_{cp} = 62.9 ºC) in each series, and their low average particle sizes indicate unimers or small micelles in solution [43, 49]. With minor additions of hydrophobic chains, micellar structures form as D_H rapidly rises from 25.9 to 47.7 nm ($PDMAEMA_{93}$-*b*-PS_{34}) and from 7.3 to 78.5 nm ($PDMAEMA_{131}$-*b*-PS_{17}). Subsequently, a transition regime in which the LCST remains relatively unaltered with increasing hydrophobic/hydrophilic ratio (r) can be observed. These regions occur between r = 0.130 and 0.756 for the $PDMAEMA_{131}$-*b*-PS_m series, and at r = 0.366 and 1.677 for the $PDMAEMA_{93}$-*b*-PS_n series. This can be explained by the consequent hindrance of the hydrophobic PS core by the hydrophilic PDMAEMA corona due to micelle formation, which stabilizes polymer/solvent interactions.

Moreover, both series show an abrupt increase in raw scattering (counts per second) when PS content exceeds 50%, strongly indicating a micelle-to-polymersome transition driven by the larger hydrophobic block [50, 51]. The same phenomenon is observed with a PDMAEMA-*b*-PAA copolymer [29]. At the same time as the aggregation transition, T_{cp} exhibits a break in its behavior and decreases abruptly. Therefore, changes in aggregation status (e.g., micelle to polymersome) seem to influence how thermal behavior responds to the copolymer's overall polarity. After micelle formation, both copolymer series also showed an increase in D_H around the compositions proposed for the micelle-to-polymersome transition based on the raw scattering (Table **2**).

The differences in where the transition regime occurs for each series can be rationalized by the environment of the thermoresponsive block (PDMAEMA) as the degree of hydration, counterion condensation, local pH and surface polarity differ between micelles and polymersomes [52–55]. Thus, LCST and T_{cp} respond not only to the overall polarity of the copolymer chain, but also to the chemical environment around the aggregate exterior. For instance, a higher surface curvature in polyelectrolyte micellar assemblies leads to reduced condensation and electrostatic repulsion between protonated units when compared to low-curvature interfaces, i.e. polymersomes [55]. Such dissimilarities in repulsion favor protonation at higher curvatures, meaning that the apparent (pK_a^{app}) of micellar surfaces is higher than in the case of polymersomes, also impacting the local pH [56]. Moreover, confinement of the apolar block creates a complex medium where polarity changes as one moves farther from the PDMAEMA-PS interface. Because these effects differ between micelles and polymersomes, the thermal behavior of a hydrophilic block is expected to differ fundamentally among free chains, micelles, polymersomes, and other aggregate types. The results presented here corroborate this hypothesis.

In Fig. **5**, the light scattering and thermal transitions (proposed micelle-to-polymersome transition) occur at different PS/PDMAEMA molar ratios for each series. This happens as the type of aggregate formed depends on the packing parameter ($P = V/a_o l_c$,) [47, 57] and not necessarily on f_{PS}:$f_{PDMAEMA}$. The packing parameter is unlikely to be directly proportional to the PS/PDMAEMA ratio. These differences may be also related to distinct hydrophilic block sizes and block copolymer molecular dispersities (Đ), which can shift morphology from vesicles to micelles through length segregation [58, 59]. Thus, the value of the packing parameter threshold for vesicle-like aggregates to form (usually 1.5) may occur at different PS/PDMAEMA ratios, as observed.

Table 2. Thermoresponsive and self-assembly characterization of PDMAEMA-*b*-PS copolymers

Material	T_{cp}(°C) [a]	Counts per second [b] (kcps)	D_H [b]	PDI [b]
$PDMAEMA_{93}$	61.0	6.4	25.9	0.465
$PDMAEMA_{93}$-*b*-PS_{34}	59.7	37.2	47.7	0.077
$PDMAEMA_{93}$-*b*-PS_{60}	60.0	47.5	48.7	0.066
$PDMAEMA_{93}$-*b*-PS_{73}	59.0	57.6	50.1	0.052
$PDMAEMA_{93}$-*b*-PS_{91}	59.7	64.7	51.3	0.061
$PDMAEMA_{93}$-*b*-PS_{113}	59.5	80.5	53.0	0.045
$PDMAEMA_{93}$-*b*-PS_{134}	58.9	112.2	56.9	0.064
$PDMAEMA_{93}$-*b*-PS_{156}	58.6	110.7	57.2	0.057
$PDMAEMA_{93}$-*b*-PS_{178}	56.6	311.7	68.3	0.024
$PDMAEMA_{93}$-*b*-PS_{305}	58.0	313.6	69.8	0.018
$PDMAEMA_{131}$	62.9	4.2	7.3	0.206
$PDMAEMA_{131}$-*b*-PS_{17}	61.0	28.0	78.5	0.238
$PDMAEMA_{131}$-*b*-PS_{36}	60.5	30.8	75.3	0.250
$PDMAEMA_{131}$-*b*-PS_{56}	60.2	55.1	64.5	0.186
$PDMAEMA_{131}$-*b*-PS_{99}	59.8	381.0	112.9	0.198
$PDMAEMA_{131}$-*b*-PS_{152}	58.2	298.4	99.1	0.128
$PDMAEMA_{131}$-*b*-PS_{253}	58.1	279.0	70.1	0.062

[a]Cloud point temperatures obtained in buffer solution via UV-Vis spectroscopy. [b] Number of counts per second, hydrodynamic diameters, and polydispersity indexes obtained via dynamic light scattering for PDMAEMA and PDMAEMA-*b*-PS copolymers.

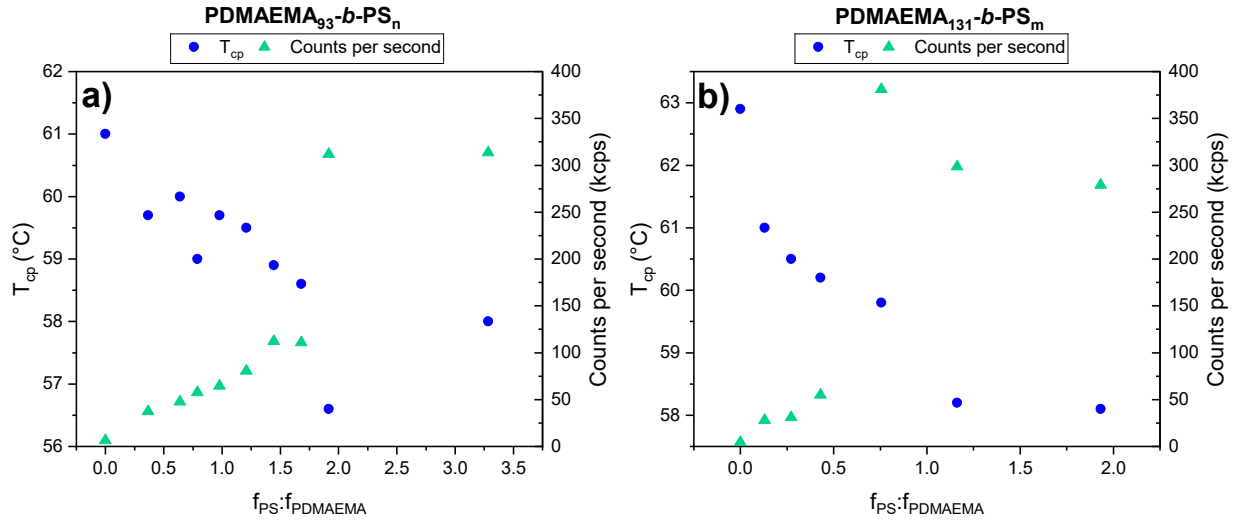


Fig. 5 T_{cp} and raw light scattering for a) $PDMAEMA_{93}$-*b*-PS_n and b) $PDMAEMA_{131}$-*b*-PS_m series in phosphate buffer solution.

Conclusion

In this study, two series of narrowly dispersed PDMAEMA-*b*-PS copolymers, each with the same hydrophilic block, were synthesized via a one-pot RAFT polymerization in bulk. Materials were structurally characterized via ^{1}H-NMR and SEC to obtain the hydrophobic/hydrophilic ratios, M_n, and Đ. All 17 (co)polymers exhibited thermoresponsive behavior through UV-Vis spectroscopy, and the cloud point temperature of PDMAEMA could be tuned between 58°C and 63°C in aqueous buffer solution. Introducing minimal hydrophobic segments into the macromolecules led to a sharp decline in T_{cp} while simultaneously increasing the hydrodynamic radii of the polymer chains, which was associated with the

appearance of micelles. Further increases in the PS fraction caused small changes in thermal response due to aggregate stability until DLS analysis showed a considerable increase in scattering intensity around r = 2 for $PDMAEMA_{93}$-*b*-PS_n and r = 0.7 for $PDMAEMA_{131}$-*b*-PS_m, indicating the formation of PDMAEMA-*b*-PS polymersomes due to an increase in the copolymer packing parameter. Thus, this work highlights how aggregation affects the thermal behavior of amphiphilic block copolymers, with a view to future stimuli-responsive applications.

CRediT authorship contribution statement

Fabio Herbst Florenzano: Conceptualization, Supervision, Project administration, Funding acquisition, Investigation, Resources, Writing – review & editing. **Vinicios Santiago Araujo**: Conceptualization, Methodology, Investigation, Formal analysis, Visualization, Writing – original draft.

Declaration of use of generative AI

During the preparation of this work the authors used ChatGPT to generate images used in this manuscript. No text was generated by AI tools. Whenever used, all information was previously checked, and the authors take responsibility for the content of the published article.

Declaration of Competing Interest

The authors have no relevant competing interests to declare regarding the content of this article.

Acknowledgements

This study was funded by the Programa Institucional de Bolsas de Iniciação Científica (PIBIC) and Fundação de Amparo à Pesquisa do Estado de São Paulo (FAPESP), process numbers 2022/15447-0 and 2022/02049-6.

References

1. Marsili L, Dal Bo M, Eisele G, et al (2021) Characterization of Thermoresponsive Poly-N-Vinylcaprolactam Polymers for Biological Applications. Polymers 13:2639. https://doi.org/10.3390/polym13162639
2. Pasparakis G, Tsitsilianis C (2020) LCST polymers: Thermoresponsive nanostructured assemblies towards bioapplications. Polymer 211:123146. https://doi.org/10.1016/j.polymer.2020.123146
3. Kira M, Citterio D, Hiruta Y (2026) Dual thermo-responsive pH-Sensitive amino acid-derived zwitterionic copolymers: Balancing electrostatic and hydrophilic interactions in LCST–UCST behavior. Polymer 352:129852. https://doi.org/10.1016/j.polymer.2026.129852
4. Xu Y, Wang S, Gao H, et al (2026) Biocompatible Thermoresponsive Hydroxypropyl Cellulose-Based Hydrogel Microspheres with Temperature-Controllable Drug Release and Lubricating Property. Biomacromolecules 27:2283–2296. https://doi.org/10.1021/acs.biomac.5c02691
5. Shahriari MH, Shaban M, Salmani H, et al (2026) Enhanced delivery of regorafenib in TPGS-based nanomicelles incorporated into hyaluronic acid-methylcellulose hydrogel against colon cancer cells. J Drug Deliv Sci Technol 121:108201. https://doi.org/10.1016/j.jddst.2026.108201
6. K. Beathard-Wojan A, Agrahari V (2026) Thermoresponsive hydrogels for controlled drug delivery to the back of the eye: a data-driven guide to formulation design. Biomater Sci. https://doi.org/10.1039/D6BM00104A
7. Doberenz F, Zeng K, Willems C, et al (2020) Thermoresponsive polymers and their biomedical application in tissue engineering – a review. J Mater Chem B 8:607–628. https://doi.org/10.1039/C9TB02052G
8. Kumar A, Nirmale P, Kondaveeti SB, et al (2026) Thermo-Sensitive Polymeric Networks for Next-Generation Wound Management: A Review. AAPS PharmSciTech 27:180. https://doi.org/10.1208/s12249-026-03423-5
9. Saverina EA, Frolov NA, Kamanina OA, et al (2023) From Antibacterial to Antibiofilm Targeting: An Emerging Paradigm Shift in the Development of Quaternary Ammonium Compounds (QACs). ACS Infect Dis 9:394–422. https://doi.org/10.1021/acsinfecdis.2c00469
10. Javadi H, Lehnen A-C, Hartlieb M (2025) Bioinspired Cationic Antimicrobial Polymers. Angew Chem Int Ed 64:e202503738. https://doi.org/10.1002/anie.202503738
11. Dong Y, Li Z, Chu X, et al (2026) Endogenous pH-responsive induced reversible switching of multifunctional properties of antibacterial cotton fabrics. Colloids Surf B Biointerfaces 265:115669. https://doi.org/10.1016/j.colsurfb.2026.115669
12. Kim H-K, Lee DY, Ganbaatar SE, et al (2026) Mechanically bactericidal and self-releasing transparent nanocone array films for multifunctional antibiofouling surfaces. Prog Org Coat 215:110107. https://doi.org/10.1016/j.porgcoat.2026.110107
13. Silva IWF, Souza VV, Florenzano FH (2022) Effect of anions, urea and aggregation state on the thermal behavior of PDMAEMA-based polymers. Colloid Polym Sci 300:1217–1221. https://doi.org/10.1007/s00396-022-05013-w
14. Zhang J, Li S, Wang Z, et al (2021) Multitunable Thermoresponsive and Aggregation Behaviors of Linear and Cyclic Polyacrylamide Copolymers Comprising Heterofunctional Y Junctions. Macromolecules 54:8229–8242. https://doi.org/10.1021/acs.macromol.1c00794
15. Klamut M, Zaborniak I, Bałbustyn J, et al (2024) Precise tailoring of thermoresponsive characteristics: Revealing ATRP opportunities for controlled poly(ethylene glycol)-based monomers composition in cyclodextrin-containing polymers. Polymer 312:127645. https://doi.org/10.1016/j.polymer.2024.127645
16. Zanata D de M, Felisberti MI (2022) Thermo- and pH-responsive POEGMA-*b*-PDMAEMA-*b*-POEGMA triblock copolymers. Eur Polym J 167:111069. https://doi.org/10.1016/j.eurpolymj.2022.111069
17. Prud MV, Kyrychenko A, Kalugin ON (2023) pH-Controllable Coating of Silver Nanoparticles with PMMA- *b* -PDMAEMA Oligomers: A Molecular Dynamics Simulation Study. J Phys Chem C 127:11748–11759. https://doi.org/10.1021/acs.jpcc.3c02779
18. Liu X, Li Z, Zhao M, et al (2026) Synthesis and characterization of nitrobenzyl carbonate (NBC)-based photodegradable amphiphilic polymers with temperature/pH/light-response. Polymer 345:129599. https://doi.org/10.1016/j.polymer.2026.129599
19. Hu L, Wang Y, Yin Q, et al (2019) Multiple morphologies of a poly(methyl methacrylate)-block-poly(N,N-dimethyl aminoethyl methacrylate) copolymer with pH-responsiveness and thermoresponsiveness. J Appl Polym Sci 136:47972. https://doi.org/10.1002/app.47972
20. Kim B, Kwon M, Mohanty AK, et al (2021) LCST and UCST Transition of Poly(DMAEMA-b-MEO2MA) Copolymer in KHP Buffer. Macromol Chem Phys 222:2000330. https://doi.org/10.1002/macp.202000330

21. de Souza VV, Carretero GPB, Vitale PAM, et al (2022) Stimuli-responsive polymersomes of poly [2-(dimethylamino) ethyl methacrylate]-b-polystyrene. Polym Bull 79:785–805. https://doi.org/10.1007/s00289-020-03533-5
22. Utievskyi Y, Neumann C, Sindlinger J, et al (2023) Polyoxometalate-Modified Amphiphilic Polystyrene-block-poly(2-(dimethylamino)ethyl methacrylate) Membranes for Heterogeneous Glucose to Formic Acid Methyl Ester Oxidation. Nanomaterials 13:2498. https://doi.org/10.3390/nano13182498
23. Vargas-Alfredo N, Santos-Coquillat A, Martínez-Campos E, et al (2017) Highly Efficient Antibacterial Surfaces Based on Bacterial/Cell Size Selective Microporous Supports. ACS Appl Mater Interfaces 9:44270–44280. https://doi.org/10.1021/acsami.7b11337
24. Staff RH, Gallei M, Landfester K, Crespy D (2014) Hydrophobic Nanocontainers for Stimulus-Selective Release in Aqueous Environments. Macromolecules 47:4876–4883. https://doi.org/10.1021/ma501233y
25. Wang X, Jiang G, Wei Z, et al (2013) Preparation and drug release property of CO2 stimulus-sensitive poly(*N*, *N*-dimethylaminoethyl methacrylate)-*b*-polystyrene nanoparticles. Eur Polym J 49:3165–3170. https://doi.org/10.1016/j.eurpolymj.2013.07.024
26. Ma D, Li H, Meng Z, et al (2021) Absolute and Fast Removal of Viruses and Bacteria from Water by Spraying-Assembled Carbon-Nanotube Membranes. Environ Sci Technol 55:15206–15214. https://doi.org/10.1021/acs.est.1c04644
27. Bondaz L, Cousin F, Muller F, et al (2021) pH-sensitive behavior of the PS-b-PDMAEMA copolymer at the air - water interface. Polymer 221:123619. https://doi.org/10.1016/j.polymer.2021.123619
28. Sun H, Chen X, Han X, Liu H Dual Thermoresponsive Aggregation of Schizophrenic PDMAEMA-b-PSBMA Copolymer with an Unrepeatable pH Response and a Recycled CO2/N2 Response
29. Han X, Zhang X, Zhu H, et al (2013) Effect of Composition of PDMAEMA-b-PAA Block Copolymers on Their pH- and Temperature-Responsive Behaviors. Langmuir 29:1024–1034. https://doi.org/10.1021/la3036874
30. Lerch A, Käfer F, Prévost S, et al (2021) Structural Insights into Polymethacrylamide-Based LCST Polymers in Solution: A Small-Angle Neutron Scattering Study. Macromolecules 54:7632–7641. https://doi.org/10.1021/acs.macromol.1c00698
31. Gjerde NS, Del Giudice A, Zhu K, et al (2023) Synthesis and Characterization of a Thermoresponsive Copolymer with an LCST–UCST-like Behavior and Exhibiting Crystallization. ACS Omega 8:31145–31154. https://doi.org/10.1021/acsomega.3c03162
32. A. Maleki, A. Kjøniksen, K. Zhu, B. Nyström (2011) Temperature-induced aggregation kinetics in aqueous solutions of a temperature-sensitive amphiphilic block copolymer. J Phys Chem B. https://doi.org/10.1021/jp202607p
33. Hu L, Zhou S, Zhang X, et al (2024) Self-Assembly of Polymers and Their Applications in the Fields of Biomedicine and Materials. Polymers 16:2097. https://doi.org/10.3390/polym16152097
34. Chiefari J, Chong YK (Bill), Ercole F, et al (1998) Living Free-Radical Polymerization by Reversible Addition−Fragmentation Chain Transfer: The RAFT Process. Macromolecules 31:5559–5562. https://doi.org/10.1021/ma9804951
35. Moad G (2016) RAFT polymerization to form stimuli-responsive polymers. Polym Chem 8:177–219. https://doi.org/10.1039/C6PY01849A
36. Corrigan N, Jung K, Moad G, et al (2020) Reversible-deactivation radical polymerization (Controlled/living radical polymerization): From discovery to materials design and applications. Prog Polym Sci 111:101311. https://doi.org/10.1016/j.progpolymsci.2020.101311
37. Eckert T, Abetz V (2020) Polymethacrylamide—An underrated and easily accessible upper critical solution temperature polymer: Green synthesis via photoiniferter reversible addition–fragmentation chain transfer polymerization and analysis of solution behavior in water/ethanol mixtures. J Polym Sci 58:3050–3060. https://doi.org/10.1002/pol.20200566
38. Wang X, Shan M, Zhang S, et al (2022) Stimuli-Responsive Antibacterial Materials: Molecular Structures, Design Principles, and Biomedical Applications. Adv Sci 9:2104843. https://doi.org/10.1002/advs.202104843
39. Moad G (2018) A Critical Assessment of the Kinetics and Mechanism of Initiation of Radical Polymerization with Commercially Available Dialkyldiazene Initiators. Prog Polym Sci 88:. https://doi.org/10.1016/j.progpolymsci.2018.08.003
40. Kim K, Ahn J, Park M, et al (2019) Molecular-Weight Distribution of Living Chains in Polystyrene Prepared by Reversible Addition–Fragmentation Chain-Transfer Polymerization. Macromolecules 52:7448–7455. https://doi.org/10.1021/acs.macromol.9b01331
41. Ikeda T, Kobayashi Y, Yamakawa M (2025) Tunable thermal conductivity in nanofluids through self-assembly of amphiphilic Janus nanoparticles. J Mol Liq 440:128958. https://doi.org/10.1016/j.molliq.2025.128958
42. Liu H, Lu H-H, Alp Y, et al (2024) Structural determinants of stimuli-responsiveness in amphiphilic macromolecular nano-assemblies. Prog Polym Sci 148:101765. https://doi.org/10.1016/j.progpolymsci.2023.101765
43. Kaushik KK, Tiwari S (2025) Thermosensitive self-assemblies: A review on structural and application aspects centred at drug delivery. Int J Pharm 683:126045. https://doi.org/10.1016/j.ijpharm.2025.126045
44. Ferreira Silva IW, Carretero GPB, Herbst Florenzano F (2024) Tailored Copolymers for Soft Templating of Silver Particles with Enhanced Antibacterial Properties
45. Sun F, Feng C, Liu H, Huang X (2016) PHEA-g-PDMAEA well-defined graft copolymers: SET-LRP synthesis, self-catalyzed hydrolysis, and quaternization. Polym Chem 7:6973–6979. https://doi.org/10.1039/C6PY01637E
46. Zhang X, Yu Z, Ma J, et al (2026) Green preparation of ultra-high molecular weight narrow-distribution polystyrene by enzymatic synthesis. Eur Polym J 242:114441. https://doi.org/10.1016/j.eurpolymj.2025.114441
47. Hocine S, Li M-H (2013) Thermoresponsive self-assembled polymer colloids in water. Soft Matter 9:5839–5861. https://doi.org/10.1039/C3SM50428J
48. Savicke M, Peciulyte L, Bendoraitiene J, et al (2025) Thermoresponsive properties of acenaphthylene-labelled chitosan-graft-poly(N-isopropylacrylamide) copolymers. Polym Bull 82:1893–1914. https://doi.org/10.1007/s00289-024-05608-z
49. Beach MA, Nayanathara U, Gao Y, et al (2024) Polymeric Nanoparticles for Drug Delivery. Chem Rev 124:5505–5616. https://doi.org/10.1021/acs.chemrev.3c00705
50. Jensen GV, Lund R, Gummel J, et al (2014) Monitoring the Transition from Spherical to Polymer-like Surfactant Micelles Using Small-Angle X-Ray Scattering. Angew Chem Int Ed 53:11524–11528. https://doi.org/10.1002/anie.201406489
51. Ali M, Bardhan S, Saha SK (2022) Polyoxyethylene Sorbitan Monolaurate induced vesicle-to-micelle transition of aqueous dimethyldioctadecylammonium bromide dispersion. J Mol Liq 348:118455. https://doi.org/10.1016/j.molliq.2021.118455
52. Ghezzi M, Pescina S, Padula C, et al (2021) Polymeric micelles in drug delivery: An insight of the techniques for their characterization and assessment in biorelevant conditions. J Controlled Release 332:312–336. https://doi.org/10.1016/j.jconrel.2021.02.031
53. Battaglia G, Ryan AJ (2006) Pathways of Polymeric Vesicle Formation. J Phys Chem B 110:10272–10279. https://doi.org/10.1021/jp060728n
54. Xu Q, Wang Y, Zheng Y, et al (2023) Polymersomes in Drug Delivery-From Experiment to Computational Modeling. Biomacromolecules 25:2114–2135. https://doi.org/10.1021/acs.biomac.3c00903
55. Gillespie DAJ, Hallett JE, Elujoba O, et al (2014) Counterion condensation on spheres in the salt-free limit. Soft Matter 10:566–577. https://doi.org/10.1039/c3sm52563e
56. Tagliazucchi M, Szleifer I (2017) 6 - Advanced Modeling of Ion Transport in Polymer and Polyelectrolyte-Modified Nanochannels and Nanopores. In: Tagliazucchi M, Szleifer I (eds) Chemically Modified Nanopores and Nanochannels. William Andrew Publishing, Boston, pp 131–203
57. Jin X, Kim D, Zhao M, et al (2026) Self-assembly of amphiphilic block copolymers containing thermoresponsive and surface-active poly(2-alkyl-2-oxazoline). Eur Polym J 249:114626. https://doi.org/10.1016/j.eurpolymj.2026.114626

58. Li X, Tang P, Qiu F, et al (2006) Aggregates in Solution of Binary Mixtures of Amphiphilic Diblock Copolymers with Different Chain Length. J Phys Chem B 110:2024–2030. https://doi.org/10.1021/jp055951j
59. Pijpers IAB, Meng F, Hest JCM van, Abdelmohsen LKEA (2020) Investigating the self-assembly and shape transformation of poly(ethylene glycol)-b-poly(D,L-lactide) (PEG-PDLLA) polymersomes by tailoring solvent-polymer interactions. Polym Chem 11:275–280. https://doi.org/10.1039/C9PY01089K

Supplementary Files

This is a list of supplementary files associated with this preprint. Click to download.

- SupplementaryInformation.docx